

Wavelength and Temperature Dependence of the Femtosecond Pump–Probe Anisotropies in the Conjugated Polymer MEH-PPV: Implications for Energy-Transfer Dynamics

Kevin M. Gaab and Christopher J. Bardeen*

Department of Chemistry, 600 South Mathews Avenue, University of Illinois, Urbana, Illinois 61801

Received: July 20, 2003; In Final Form: January 13, 2004

Energy transfer in the conjugated polymer poly[2-methoxy-5-(2'-ethylhexyloxy)-1,4-phenylenevinylene] (MEH-PPV) is investigated using femtosecond degenerate pump–probe experiments at 298 and 4 K. The polarization anisotropy decays are of the form $\exp[-(t)^{1/2}/T_{\text{pol}}]$, as predicted by theories of energy transfer in dilute chromophoric systems. At 4 K, these decays depend on the excitation wavelength, with $T_{\text{pol}} = 26 \text{ fs}^{-1/2}$ at the peak of the absorption (520 nm) and $T_{\text{pol}} = 78 \text{ fs}^{-1/2}$ at the low-energy side of the absorption (580 nm). This wavelength dependence becomes less pronounced at higher temperatures but is always present. We find that models for Förster energy transfer in dilute chromophore solutions cannot describe our data using a single energy-transfer rate calculated from the Förster overlap of the steady-state absorption and emission spectra. The Förster radius R_0 obtained from fitting the experimental anisotropy decays does not agree with that obtained from the steady-state absorption and fluorescence spectra. This fact, along with the wavelength dependence of the anisotropy decays, indicates that the steady-state spectral properties alone are insufficient to explain the energy-transfer properties of MEH-PPV. By use of a simple model to account for inhomogeneous broadening, vibrational line shape, and the intramolecular Stokes shift, we obtain semiquantitative agreement with the experimental results. The key quantity in this modeling is the ratio of inhomogeneous to homogeneous broadening. As the temperature increases, this ratio decreases, leading to less wavelength dependence in the anisotropy decays. The agreement between our modeling and the data suggests that models developed to describe incoherent energy transfer in dilute solutions may be useful for predicting the energy-transport properties of amorphous conjugated polymers, as long as they are modified to take factors such as vibrational structure and inhomogeneous broadening into account.

Introduction

Organic conjugated polymers are materials with great technological potential. Of the many applications envisioned for these materials, many involve the absorption and emission of light. Examples include optical sensors,¹ light-emitting diodes,² and solar cells.³ Such applications depend on the dynamics of excited states (excitons) in these polymers. An excited chromophore can not only undergo nonradiative relaxation to its ground state but can also transfer its electronic energy to another chromophore in the material, resulting in energy transport or diffusion. For example, the efficiency of an organic solar cell depends on the ability of a newly created exciton to migrate to a charge-separation site within its lifetime, so that it can dissociate into charge carriers and generate photocurrent. In this instance, faster exciton migration leads to a higher yield of carriers and a more efficient solar cell. Alternatively, in light-emitting diodes, exciton migration is believed to be detrimental to device operation, since exciton migration to quenching defects is thought to limit electroluminescence efficiency. Thus, an improved understanding of energy transport, or exciton diffusion, in these polymers is important in terms of being able to design better materials.

The simplest model for energy transfer in molecular materials is the Förster model, which assumes incoherent energy transfer between two molecules separated by a distance R , which interact

via a dipole–dipole mechanism. The incoherent dipole–dipole coupling leads to a $1/R^6$ dependence for the transfer rate.⁴ This model has successfully described electronic energy transfer in a great variety of systems, from labeled proteins to concentrated dye solutions. Application of the Förster model to a system consisting of only a single donor species allows one to generate a detailed model for the energy transfer and to predict various experimental quantities, such as the exciton diffusion constant.⁵ It is then of great interest to determine how accurately energy-transfer dynamics in conjugated polymers can be described in terms of standard Förster-type models. Various factors may complicate the application of such models to real polymeric systems. Such complications include the small distances between chromophores (on the order of a few Angstroms, small compared to molecular dimensions of tens of Angstroms) which preclude the use of the point dipole model,⁶ the amount of local disorder (both energetic and orientational),^{7–10} and the possibility that energy transfer occurs on a time scale faster than intramolecular vibrational relaxation (hot transfer).¹¹ All these factors may be taken into account to at least some degree by modifications of the standard Förster model. One last possibility is that the assumption that the chromophores are localized on individual chain segments is incorrect, and the intermolecular interaction is strong enough to generate new, Frenkel exciton states that are delocalized over multiple chromophores. In this limit, the Förster model breaks down completely and the transport is described by a more complicated model that takes coherence effects into account.^{12,13}

* Author to whom correspondence may be addressed. E-mail: bardeen@scs.uiuc.edu.

In this paper, we want to concentrate on more disordered systems where the Förster model is most likely to be valid. The conjugated polymer we study is poly[2-methoxy-5-(2'-ethyl-hexyloxy)-1,4-phenylenevinylene] (MEH-PPV), a well-known phenylene-vinylene polymer whose alkoxy sidegroups give it enhanced solubility and also render it amorphous in the solid state.^{14,15} Since its steady state absorption and emission spectra are virtually unchanged in going from dilute solution to the solid phase, there is no evidence that new, interchromophore exciton states are formed in the solid. On the other hand, the fluorescence dynamics do change upon going from the dilute solution to the solid, and there is evidence for the formation of new, low energy trapping states such as excimers.^{16,17} But these phenomena do not dominate the spectroscopy of MEH-PPV at early times, and to a first approximation, this polymer may be thought of as a highly concentrated, frozen solution of individual phenylene-vinylene chromophores with varying conjugation lengths. We use femtosecond degenerate pump-probe spectroscopy to study the anisotropy decay of the ground-state bleach in MEH-PPV, which is directly related to the probability of energy transfer from an initially excited chromophore to a different, randomly oriented neighbor. We find that the observed decay depends on the excitation wavelength, which indicates that the transport is dispersive. In other words, depending on where in the absorption band we excite, the energy-transfer dynamics are different due to the inhomogeneous distribution of chromophore energies. This dispersive transport is emphasized at low temperatures, where the ratio of inhomogeneous to homogeneous broadening increases. The anisotropy decay rates do not change as much as would be expected from the large thermochromic shifts in the absorption and fluorescence spectra, which reduce the steady-state Förster overlap by an order of magnitude. Both observations indicate that understanding the initial energy transfer in MEH-PPV requires a modified Förster model that treats both the homogeneous and inhomogeneous broadening, as well as the instantaneous vibrational Stokes shift. This model cannot predict the time-dependent fluorescence shifting in conjugated polymers over the entire excited-state lifetime, but does explain the early-time energy transfer that determines the decay rate of the pump-probe anisotropy. The advantage of the present approach is that it allows for direct contact with analytical theories that predict spatial diffusion, which is ultimately the quantity of interest from the point of view of technological applications. Our observation that the dispersive energy transfer is not washed out by homogeneous broadening even at room temperature demonstrates that the heterogeneity of the material must be taken into account when modeling the characteristics of conjugated materials under ambient conditions.

Experimental Section

The samples are prepared by dissolving 5–7 mg/mL of MEH-PPV (Sigma-Aldrich, average $M \approx 51\,000$) in methylene chloride. The resulting solutions are stirred at room temperature for several days and then spin cast onto 1 mm thick glass substrates at 600 rpm for 600 s to yield films with a peak optical density of between 0.5 and 1.0. The thin films are immediately loaded into a cryostat and placed under vacuum to prevent photo-oxidative damage.

Steady-state absorption spectra were taken using an Ocean Optics S-2000 UV-vis spectrometer. Steady-state fluorescence spectra were taken using a 150-W Hg lamp, with the output passed through a monochromator and reflected off a dichroic mirror to select the excitation wavelength. The excitation and

collection was set up in a confocal arrangement normal to the sample surface. The fluorescence was collected after the dichroic, coupled into a 400 μm diameter UV-vis optical fiber, and detected with the CCD from the Ocean Optics spectrometer.

Both the time-resolved fluorescence and pump-probe experiments utilize a regeneratively amplified Ti-Sapphire laser system which generates ~ 100 -fs pulses, centered at 800 nm, at a 40-kHz repetition rate. The output of this system is used to pump a noncollinear optical parametric amplifier (NOPA), as has been described elsewhere.^{18–20} The output of the NOPA is tunable from ~ 480 to ~ 750 nm. The generated visible pulse has a bandwidth of ~ 16 – 20 nm, as measured using an Ocean Optics S2000 spectrometer. The pulse is then passed through a prism compressor. The intensity autocorrelation is measured in the cryostat by detecting fluorescence generated by the two-photon absorption of *p*-terphenyl in a PMMA film, yielding autocorrelation widths of 30–40 fs. The validity of these autocorrelations was verified by comparing the results at 600 nm with those obtained from second harmonic generation in a 0.1-mm BBO crystal.

The time-resolved fluorescence measurements are taken using excitation pulses centered at 513 nm, with an excitation fluence at the sample of $\sim 1\ \mu\text{J}/\text{cm}^2$. The fluorescence is detected by a streak camera (Hamamatsu Streakscope), which allows the simultaneous measurement of both the spectrum and decay. The instrumental response for the streak camera is ~ 20 ps. For the pump-probe experiments, the NOPA output is split to generate the pump and probe pulses, with the latter delayed using a mechanical translation stage with 0.1- μm resolution. Both the pump and probe pulses pass through calcite polarizers, with the polarization of the probe pulse oriented at 45° relative to that of the pump. The beams are focused in a noncollinear geometry by a single lens. A polarizer after the sample separates the parallel and perpendicular components of the probe beam, which are then detected using silicon photodiodes. Standard lock-in and subtraction techniques are used to improve the signal-to-noise ratio. The excitation fluence at the sample is $\sim 20\ \mu\text{J}/\text{cm}^2$, resulting in a maximum differential transmittance $\Delta T/T$ of 10^{-2} at 500 nm. When exciting at these fluence levels near the absorption maximum, we observe an intensity dependence in the short-time dynamics of both the perpendicular and parallel polarizations of the pump-probe decay.²¹ However, the dynamics of the anisotropy decay are power independent over nearly 2 orders of magnitude, suggesting that the mechanism giving rise to this power dependence is isotropic, affecting both polarizations equally. Therefore it does not fundamentally affect the picosecond anisotropy decays.

Results and Discussion

In Figure 1a, we compare the absorption and emission spectra of dilute MEH-PPV in toluene solution and in a neat polymer film. The spectra are similar, with some additional broadening of the absorption and a shift of the fluorescence observed in the neat film. The shifting is most likely due to a solvatochromic effect where the highly polarizable polymer environment lowers the energy of the emitting state relative to the toluene solution. The broadening of the absorption is likely due to the fact that in the solid phase inhomogeneous broadening becomes more pronounced due to a larger distribution of static environments. As the temperature is lowered, both the absorption and emission of the neat film undergo a shift to longer wavelengths and sharpen somewhat. The absorption and fluorescence shift unequally, however, and this, along with the spectral sharpening, leads to a decrease in their spectral overlap. This is shown in

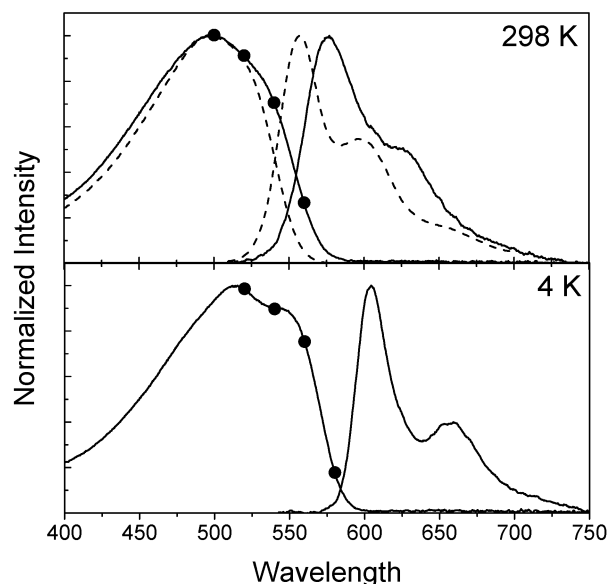


Figure 1. Steady state absorption and emission spectra for MEH-PPV thin film (solid line) and dilute solution in toluene (dashed line). Excitation wavelengths (●) for the pump–probe experiments are shown on the absorption spectra.

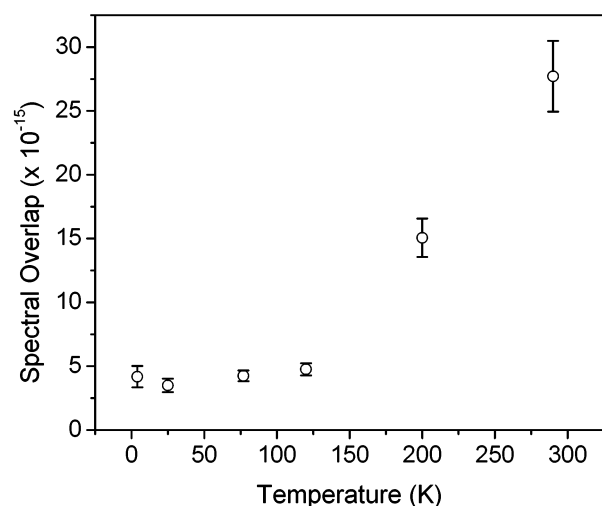


Figure 2. Temperature-dependent steady-state spectral overlap, $\int d\nu \epsilon(\nu)f(\nu)/\nu^4$.

Figure 2, which plots the integrated overlap of the absorption and emission as a function of temperature. As the temperature decreases to 4 K, the overlap decreases by almost 1 order of magnitude, mainly due to the fact that the fluorescence shifts more than the absorption. This spectral overlap is one of the components that goes into calculating the usual Förster rate for energy transfer^{4,22}

$$k_{\text{ET}} = \frac{1}{\tau_{\text{fl}}} \frac{R_0^6}{R^6} \quad (1a)$$

$$R_0^6 = \frac{9000 \ln(10) \phi_{\text{fl}} \kappa^2}{128 \pi^5 N_A n^4} \int_0^\infty \epsilon(\nu) f(\nu) \frac{d\nu}{\nu^4} \quad (1b)$$

where R is the separation between chromophores, n is the index of refraction, τ_{fl} is the fluorescence lifetime of the donor (which in this case is identical to the acceptor), ϕ_{fl} is the quantum yield, κ^2 is an orientation factor, N_A is Avogadro's number, $\epsilon(\nu)$ is the absorption spectrum, and $f(\nu)$ is the fluorescence spectrum

whose integral has been normalized to 1. R_0 combines these factors into a single length called the critical Förster radius. From eq 1, the decrease in the steady-state spectral overlap predicts an order of magnitude decrease in k_{ET} between the MEH-PPV chromophore segments at 4 K.

To test this prediction, we measured the time-dependent pump–probe anisotropy decay. In a sample where the chromophores are randomly oriented and unable to rotate, energy transfer between the chromophores serves to randomize the orientational distribution of the excited molecules. This randomization can be monitored as the decay of the polarization anisotropy in a signal that probes the excited-state population.²³ In this paper, we use a degenerate pump–probe experiment to measure the depolarization of the ground-state bleach, an experiment that has been used widely in studying the dynamics of energy transfer in biological light-harvesting complexes.^{24–27} As the excited-state population moves to a different site, the ground-state bleach is also transferred and loses its polarization memory. The excited-state anisotropy decay $r(t)$ is directly proportional to $G_S(t)$, the probability that an excited state residing on a particular site at time $t = 0$ still remains on that site at a later time t .²³ $G_S(t)$, in turn, can be related to the energy transfer properties of the system in the Förster limit^{28–30}

$$r(t) = G_S(t) = \exp[-C\lambda^{-1/2}\gamma\Gamma((1/2))(t/\tau_{\text{fl}})^{1/2}] \quad (2a)$$

$$C = \frac{4}{3} \pi R_0^3 \rho \quad (2b)$$

In eq 2b, R_0 is the Förster radius defined in eq 1b, ρ is the number density of chromophores, $\Gamma(x)$ is the gamma function, γ is a factor that takes orientational disorder into account, and τ_{fl} is the excited-state lifetime. λ is either 1 or 2 depending on whether the system is in the limit of donor–donor transfer and back transfer is possible ($\lambda = 2$) or whether the transfer is irreversible and the acceptors act as traps ($\lambda = 1$). We have also assumed the transfer can occur in three dimensions. The dependence of $G_S(t)$ on the Förster radius results from C , the number of possible acceptors within the Förster radius, and predicts that the anisotropy decay rate is proportional to the square root of the spectral overlap. Assuming that the R_0 value is determined by the steady-state spectral overlap, the data in Figure 2 indicate that the decay rate of $G_S(t)$ should decrease by a factor of about 3 from 298 to 4 K. A second assumption of eq 2a is that all chromophores are isoenergetic, with no inhomogeneous broadening. Thus varying the excitation energy only changes the probability of creating an excited state, and the anisotropy decay of that state should be the same for all excitation wavelengths.

The data in Figure 3 show that neither of the above assumptions is correct for MEH-PPV. We measure both parallel and perpendicular probe signals at several wavelengths in the absorption band. In spin-cast MEH-PPV, the polymer chains lie preferentially in the plane of the film, and in this case of a planar film, the correct definition of the anisotropy is³¹

$$r(t) \equiv \frac{S_{\parallel}(t) - S_{\perp}(t)}{S_{\parallel}(t) + S_{\perp}(t)} \quad (3)$$

Working up the data according to the definition of the anisotropy for a three-dimensional system does not change the data fits in any important way. We find that in solid MEH-PPV, the anisotropy decay is very rapid, on the order of 1 ps, and nonexponential. At all wavelengths, the initial anisotropy ranges from 0.45 to 0.48, close to the ideal value of 0.50. At both 298

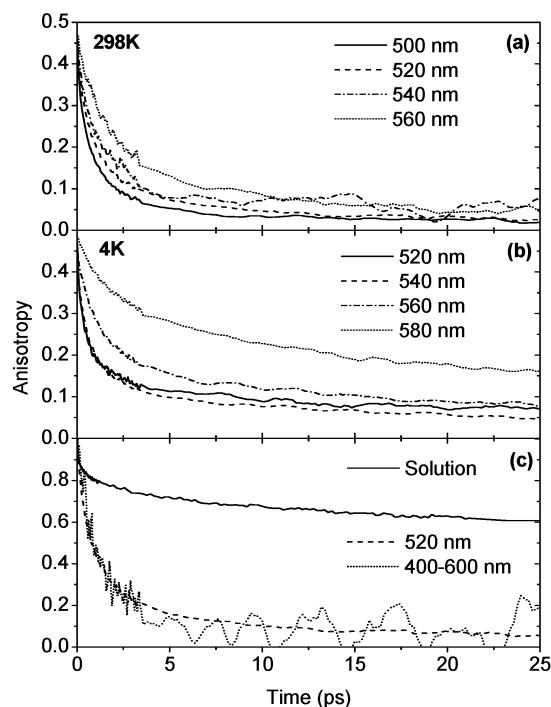


Figure 3. Degenerate pump-probe anisotropy decays for thin films, with excitation wavelengths shown in Figure 1. Decays at 298 K (a) are shown for excitations at 500 nm (solid line), 520 nm (dashed line), 540 nm (dot-dashed line), and 560 nm (dotted line). Decays at 4 K (b) are for excitations at 520 nm (solid line), 540 nm (dashed line), 560 nm (dot-dashed line), and 580 nm (dotted line). Panel c gives a comparison of the normalized decays for a toluene solution (solid line) and the thin film 520 nm (dashed line) and 400–600 nm (dotted line) decays.

K (Figure 3a) and 4 K (Figure 3b), the anisotropy decay varies substantially with wavelength, getting more rapid as the excitation is tuned toward the absorption peak. But although there is a pronounced wavelength dependence, the temperature dependence is relatively weak and nonexistent at the shorter wavelengths. In Figure 3c, we compare the normalized room-temperature anisotropy decay for MEH-PPV in toluene, similar to what was observed by Schwartz and co-workers,³² to that of MEH-PPV in the solid state. Also shown in Figure 3c is the anisotropy decay of the transient emission of MEH-PPV at 600 nm after pumping at 400 nm, which is identical to that observed at 500 and 520 nm in the degenerate pump-probe experiment. This result demonstrates that probing the bleach polarization is equivalent to probing the emission polarization and is not measurably perturbed by complicating factors such as excited-state absorption.

None of the data in Figure 3 can be fit with a single-exponential decay. A double exponential, with four adjustable parameters, resulted in good fits to the data, but the physical origin of the wavelength variation is unclear. Fitting the data with a stretched exponential function resulted in power laws of ~ 0.5 at all wavelengths, which suggested using the general function

$$r(t) = A \exp\left[\frac{-(t)^{1/2}}{T_{\text{pol}}}\right] + y_0 \quad (4)$$

to fit the data, which has only three adjustable parameters, A , T_{pol} , and y_0 . The advantage of eq 4 is that it has the same form as the theoretical prediction eq 2a, and thus we can use it to connect our results to that previously developed theory of energy

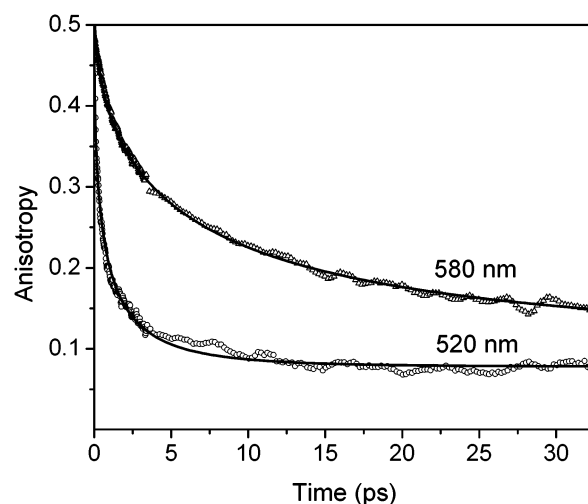


Figure 4. Experimental pump-probe anisotropy decays at 4 K for excitations at 520 nm (○) and 580 nm (△) and the best fits for each data set (solid line).

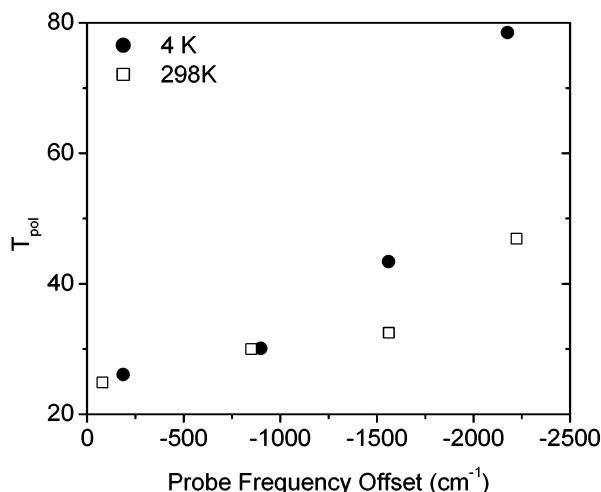


Figure 5. Anisotropy decay rate, T_{pol} , at 298 K (□) and 4 K (●) determined from best fits to the experimental decays. Excitation wavelengths are plotted as a shift from the absorption maximum ($\sim 20\,080\text{ cm}^{-1}$ at 298 K and $\sim 19\,420\text{ cm}^{-1}$ at 4 K).

transfer in a disordered medium. Fits to the data using eq 4 are shown in Figure 4 for anisotropies at 520 and 580 nm at 4 K. At all temperatures and wavelengths, the offset to the anisotropy y_0 was not 0 but ranged between 5 (at 298 K) and 20% (at the longest wavelength at 4 K) of the initial amplitude A . This offset is too large to be the result of residual back transfer, which is predicted to give an offset of at most a few percent.³¹ Its origin is unclear, and it does not vary systematically enough with wavelength to extract a definite trend. More straightforward to analyze is the decay time T_{pol} , which can be directly related to the decay time of $G_S(t)$ in eq 2. The variation of T_{pol} with wavelength is plotted in Figure 5 for our data at both 298 and 4 K. All the points are plotted relative to the absorption maximum, which shifts to longer wavelengths by about 20 nm as the temperature is decreased to 4 K. In this plot, we can clearly see both the wavelength dependence and the temperature dependence, which is significant only for the low-energy side of the absorption.

Two aspects of our data are in qualitative disagreement with the simple Förster approach to energy transfer. First, the expected slow in the transfer, due to poor overlap of the absorption and emission at 4 K, is only observed for wavelengths

TABLE 1: Anisotropy Decay Rates and Corresponding Förster Radii Compared with Radii Calculated from the Steady State

	excitation (nm)	T_{pol} (fs ^{-1/2})	R_0^{anis} (nm)	R_0^{ss} (nm)
298 K	500	24.9	1.40	2.59
	520	30.0	1.32	
	540	32.5	1.28	
	560	46.9	1.14	
4 K	520	26.1	1.52	1.89
	540	30.1	1.45	
	560	43.4	1.28	
	580	78.5	1.05	

on the red edge of the absorption. Even here, the change in T_{pol} is significantly less than the factor of 3 predicted based on the data in Figure 2. Near the absorption peak, the anisotropy decays are temperature independent to within the experimental error. The absence of the strong temperature dependence expected from the overlap of the steady-state absorption and fluorescence suggests this is not the right quantity for predicting the energy transfer rates. This can be seen by extracting an effective R_0 from our data using eq 2. By use of a number density $\rho = 10^{21} \text{ cm}^{-3}$,³³ a fluorescence lifetime τ_{fl} of 200 ps at 298 K and 350 ps at 4 K (exponential fits to decays measured in our lab), $\lambda = 1$, $\gamma = 0.8452$,³¹ and our experimental values for T_{pol} , we obtain the Förster radii for various excitation wavelengths given in Table 1. The R_0 's calculated from the steady-state spectra at these temperatures are also given. To calculate these values, eq 1b was used with the parameters $n = 1.7$,³⁴ $\kappa^2 = 0.6901$ (static, randomly oriented molecules),³¹ a peak $\epsilon = 36\,000$ at 500 nm,³⁵ and a quantum yield of 0.15.³⁶ The steady-state R_0 's do not agree with those obtained from the dynamic measurements, being a factor of 1.4–2.3 larger at both 298 and 4 K. As will be discussed below, the actual emission spectrum that determines the initial anisotropy decay is probably the vibrationally Stokes-shifted emission prior to further relaxation. The spectral overlap of this early-time, higher-energy emission should be greater than that of the fully relaxed fluorescence, however, leading to even larger R_0 's. The calculated R_0 's are relatively insensitive to errors in quantities such as n and ϵ , since it only depends on them raised to the $1/6$ power. Similarly, uncertainties in ρ and T_{pol} have a small effect on the R_0 calculated from eq 2. One origin of the discrepancy could be the point-dipole approximation inherent in eq 1. When the separation of chromophores becomes less than the molecular radius, the point-dipole approximation is no longer valid and in general overestimates the Coulombic interaction that leads to the Förster energy-transfer rate.^{6,37} A more accurate calculation of the energy transfer would involve taking the extended structure of the chromophores into account.³⁸ A second explanation for the discrepancy could be the breakdown of eq 2 at high chromophore density, although it is expected to be accurate to fairly high densities.²⁸ A final complication is the fact that some local order may exist in MEH-PPV,³⁹ invalidating the assumption of perfectly randomized chromophores inherent in eq 2.

It is instructive to look at the effects of the differing values for R_0 on the estimation of the exciton diffusion constant in MEH-PPV. The diffusion coefficient in this simple limit is given by

$$D = A \frac{R_0^2}{\tau_{\text{fl}}} C^{4/3} = A \left(\frac{4\pi\rho}{3} \right)^{4/3} \frac{R_0^6}{\tau_{\text{fl}}} \quad (5)$$

where all the constants have been previously defined and A ranges between 0.30 and 0.50.^{5,9,28,40,41} If we consider room

temperature and compare the $R_0 = 1.40$ nm from the anisotropy decay at 500 nm and the steady-state $R_0 = 2.59$ nm, this leads to calculated D s differing by a factor of ~ 40 . If we consider the three-dimensional diffusion length, given by

$$L = (6D\tau_{\text{fl}})^{1/2} = \left(6A \left(\frac{4\pi\rho}{3} \right)^{4/3} R_0^6 \right)^{1/2} \quad (6)$$

we find a factor of 6.3 difference. Using $A = 0.35$ and $\rho = 10^{21} \text{ cm}^{-3}$, we would estimate an exciton diffusion length of 10 nm from the anisotropy decays, as compared to 66 nm from the room temperature spectral overlap. While the actual diffusion lengths may be different from these crude estimates, this difference in estimated diffusion lengths illustrates the importance of determining an accurate value for the effective energy-transfer rate, which in this theoretical treatment depends sensitively on R_0 .

The second aspect of our data that is inconsistent with the simplest Förster picture is the fact that a single $G_S(t)$ is insufficient to describe the full wavelength dependence of the energy transfer. To reproduce at least the qualitative trends in our data, it is necessary to use a model that takes both the intramolecular Stokes shift and inhomogeneous broadening into account. It is similar to a model Struve and co-workers used to analyze energy transfer in the light-harvesting complex²⁵ but differs from other models for dispersive transport, which have been based either on numerical Monte Carlo simulations^{42,43} or on the linear variation of the λ parameter in the expression for $G_S(t)$.⁴⁴ We do not try to model the detailed absorption spectrum of MEH-PPV but rather try to capture the essential physical processes that underlie the observed temperature and wavelength dependence of T_{pol} . We consider an inhomogeneously broadened absorption line that consists of a Gaussian distribution of homogeneous line shapes. The homogeneous line shape is taken to be a double-peaked Gaussian to mimic the vibronic spectrum of the chromophore as deduced from its narrowed fluorescence spectrum. If the homogeneous line shape at frequency ω_i is given by

$$\text{Hom}(\omega) = \frac{1}{\sigma_h(\pi)^{1/2}} \exp \left[\frac{-(\omega_i - \omega)^2}{\sigma_h^2} \right] + \frac{A}{\sigma_h(\pi)^{1/2}} \exp \left[\frac{-(\omega_i + \omega_{\text{vib}} - \omega)^2}{\sigma_h^2} \right] \quad (7)$$

and the inhomogeneous distribution is given by

$$\text{Inho}(\omega) = \frac{1}{\sigma_i(\pi)^{1/2}} \exp \left[\frac{-(\omega_0 - \omega)^2}{\sigma_i^2} \right] \quad (8)$$

then the full absorption line shape is just the convolution of these two

$$\text{abs}(\omega) = \frac{\mu_A^2}{(\pi(\sigma_h^2 + \sigma_i^2))^{1/2}} \left\{ \exp \left[\frac{-(\omega_0 - \omega)^2}{\sigma_h^2 + \sigma_i^2} \right] + A \exp \left[\frac{-(\omega_0 + \omega_{\text{vib}} - \omega)^2}{\sigma_h^2 + \sigma_i^2} \right] \right\} \quad (9)$$

The laser frequency ω_{ex} excites a distribution of absorbers at $\{\omega_i\}$, each of which undergoes a constant Stokes shift Δ_{ss} due to intramolecular vibrational relaxation. Assuming narrow-band laser excitation, the distribution of fluorescent

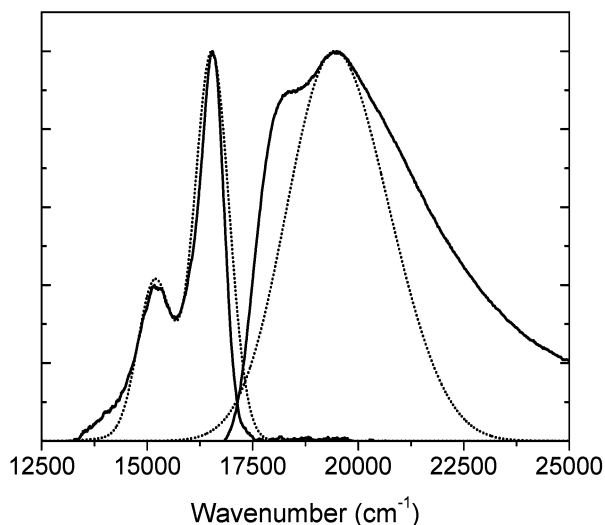


Figure 6. Comparison of the calculated absorption and emission spectra (dotted line) with the experimental spectra (solid line).

states is narrower than the full inhomogeneous distribution and is given by

$fl(\omega) =$

$$\begin{aligned} & \frac{\mu_E^2}{\pi\sigma_h(2\sigma_i^2 + \sigma_h^2)^{1/2}} \left\{ \exp \left[\frac{-\sigma_i^2}{(2\sigma_i^2 + \sigma_h^2)} \left(\frac{(\omega_{ex} - \Delta_{ss} - \omega)^2}{\sigma_h^2} + \frac{(\omega_0 - \Delta_{ss} - \omega)^2}{\sigma_i^2} + \frac{(\omega_0 - \omega_{ex})^2}{\sigma_i^2} \right) \right] + \dots \right. \\ & A \exp \left[\frac{-\sigma_i^2}{(2\sigma_i^2 + \sigma_h^2)} \left(\frac{(\omega_{ex} - \omega_{vib} - \Delta_{ss} - \omega)^2}{\sigma_h^2} + \frac{(\omega_0 - \Delta_{ss} - \omega)^2}{\sigma_i^2} + \frac{(\omega_0 - \omega_{ex} + \omega_{vib})^2}{\sigma_i^2} \right) \right] + \dots \\ & A \exp \left[\frac{-\sigma_i^2}{(2\sigma_i^2 + \sigma_h^2)} \left(\frac{(\omega_{ex} - \omega_{vib} - \Delta_{ss} - \omega)^2}{\sigma_h^2} + \frac{(\omega_0 - \omega_{vib} - \Delta_{ss} - \omega)^2}{\sigma_i^2} + \frac{(\omega_0 - \omega_{ex})^2}{\sigma_i^2} \right) \right] + \dots \\ & \left. A^2 \exp \left[\frac{-\sigma_i^2}{(2\sigma_i^2 + \sigma_h^2)} \left(\frac{(\omega_{ex} - 2\omega_{vib} - \Delta_{ss} - \omega)^2}{\sigma_h^2} + \frac{(\omega_0 - \omega_{vib} - \Delta_{ss} - \omega)^2}{\sigma_i^2} + \frac{(\omega_0 - \omega_{ex} + \omega_{vib})^2}{\sigma_i^2} \right) \right] \right\} \quad (10) \end{aligned}$$

Figure 6 shows the calculated absorption and fluorescence spectra for the parameters $\omega_0 = 19\,200\text{ cm}^{-1}$, $\sigma_i = 1374\text{ cm}^{-1}$, $\sigma_h = 416\text{ cm}^{-1}$, $\Delta_{ss} = 875\text{ cm}^{-1}$, $\omega_{vib} = 1350\text{ cm}^{-1}$, and $A = 0.4$, along with the experimental MEH-PPV spectra at 4 K. There is good agreement with the narrowed emission, but this simple model clearly does not capture the complexity of the absorption, since the strong inhomogeneous broadening washes out all recognizable vibronic features. The actual absorption line shape of MEH-PPV probably involves additional vibronic progressions,⁴⁵ a more complicated inhomogeneous distribution where different frequency components have different line shapes,⁴⁶ and may also involve vibrational frequency changes

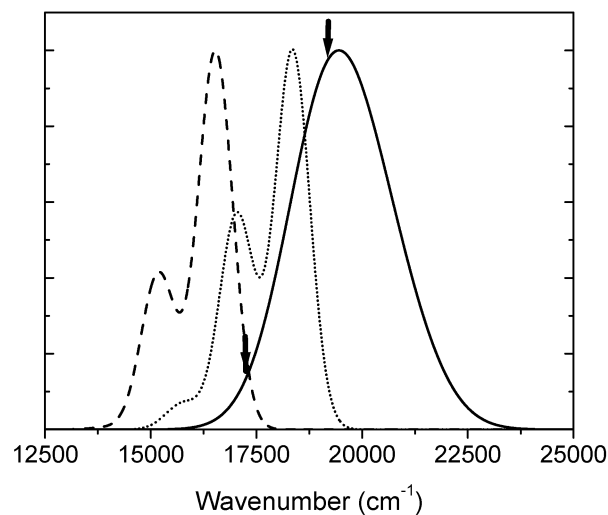


Figure 7. Emission spectra for excitation at 17 241 cm^{-1} (dotted line) and 19 231 cm^{-1} (dashed line) for the absorption spectrum (solid line) shown in Figure 6. The arrows indicate the excitation wavelengths.

in the excited state.⁴⁷ Nevertheless, this simple model manages to capture the essence of the dispersive transport, as we show below.

Figure 7 shows an example of two different fluorescence spectra obtained by excitation at 17 500 and 19 000 cm^{-1} respectively. It should be emphasized that these spectra are the initial emission spectra after vibrational relaxation but before significant energy transfer has occurred. A given molecule, whose absorption is centered at ω_i and whose Stokes shifted emission starts out at $\omega_i - \Delta_{ss}$, now sees an inhomogeneous distribution of surrounding acceptor chromophores. The decay of $G_S(t)$ is determined by C , the number of acceptors within R_0 . We can calculate C by taking advantage of its dependence on the Förster spectral overlap. The overlap between the inhomogeneously broadened absorption line shape and the narrowed emission is given by

$$\text{ovlp} = \int_{-\infty}^{\infty} \text{abs}(\omega) fl(\omega) \frac{d\omega}{\omega^4} \quad (11)$$

From eqs 1b and 2b, it can be shown that the acceptor density C is related to the overlap via

$$C = \frac{4}{3} \pi \rho \left(\frac{9000 \ln(10) \kappa^2}{128 \pi^5 N_A n^4} \int_0^{\infty} \text{abs}(\omega) fl(\omega) \frac{d\omega}{\omega^4} \right)^{1/2} \propto (\text{ovlp})^{1/2} \quad (12)$$

Plugging eq 12 into eq 2a and comparing with eq 4 yields the decay rate

$$\frac{1}{T_{\text{pol}}} = C \lambda^{-1/2} \gamma \Gamma\left(\frac{1}{2}\right) \tau_{\text{fl}}^{-1/2} \propto (\text{ovlp})^{1/2} \quad (13)$$

The overlap integral can be evaluated numerically, and the results shown in parts a and b of Figure 8 for 4 and 298 K, respectively, demonstrate the frequency dependence of T_{pol} due to the changing overlap seen in Figure 7. In Figure 8a, we have included two other calculated curves to show the sensitivity of the frequency dependence on the ratio of homogeneous to inhomogeneous broadening. As the excitation is tuned to the low-energy side of the absorption, Figure 8a shows that the dependence on σ_h becomes very dramatic, whereas near the absorption center, the decay rate only changes by 20% or less even when the ratio of homogeneous to inhomogeneous

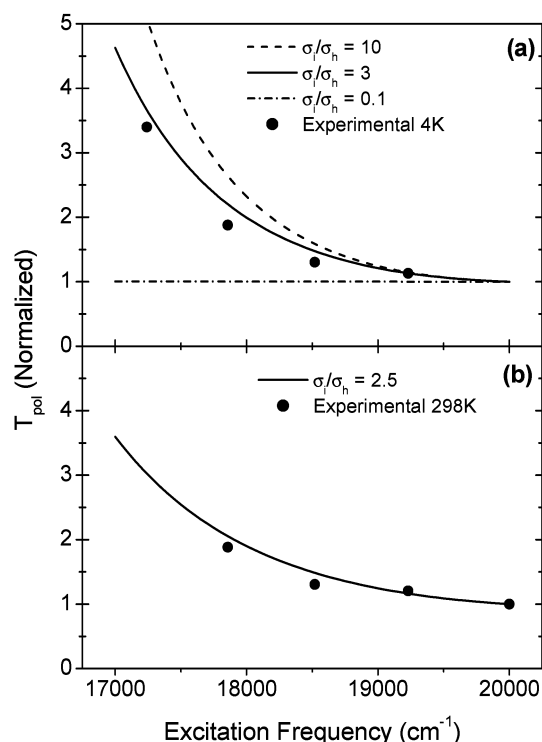


Figure 8. Calculated anisotropy decay rates (solid line) and comparison to the experimental rates (●) at 4 K (a) and 298 K (b). Decays are calculated for intermediate values of σ_i/σ_h , which reproduced the experimental spectra well. The homogeneous (dashed line) and inhomogeneous (dot-dashed line) limits are also shown.

broadening changes by an order of magnitude. As seen experimentally in MEH-PPV, the frequency dependence of the $G_S(t)$ decay is very pronounced for excitation on the low-energy wing of the absorption but falls off as the laser is tuned to the center of the absorption band. The frequency dependence in Figure 8a can be understood simply in terms of the higher density of potential acceptors when the initially excited molecule's Stokes shift does not carry its emission sufficiently far from the absorption. If the absorption were entirely homogeneously broadened, then the Stokes shift and thus the overlap of the emission and absorption would always be the same and the dependence of the decay on excitation wavelength would vanish. Such a decreased sensitivity to the excitation energy can be seen in Figure 8b, where the room-temperature T_{pol} values are plotted, along with the theoretical curve for $\sigma_i/\sigma_h = 2.5$ instead of 3.0. From inspection of Figure 1, we see that the width of the fluorescence peaks increases by approximately a factor of 2 from 4 K to room temperature, slightly more than expected from our modeling of T_{pol} .

The calculations presented in Figures 6–8 provide a semi-quantitative estimate for the parameters needed to model energy transfer in MEH-PPV and illustrates the physical origin of the trends observed experimentally in MEH-PPV with both temperature and wavelength. The trend of σ_i/σ_h with temperature is what is expected; higher temperatures lead to more homogeneous broadening, and as mentioned above, this agrees reasonably well with what is observed in the spectral line shapes. Given our assumptions, one question is whether $\sigma_i/\sigma_h = 3$ at 298 K is close to the actual value. If our assumptions outlined above are correct, then the ratios from Figure 8 are within 30% of the actual value, from varying our fit parameters. The model can be improved, however, by relaxing some of those assumptions. As mentioned above, a more realistic model would treat the detailed vibronic structure of MEH-PPV^{45,46} and take into

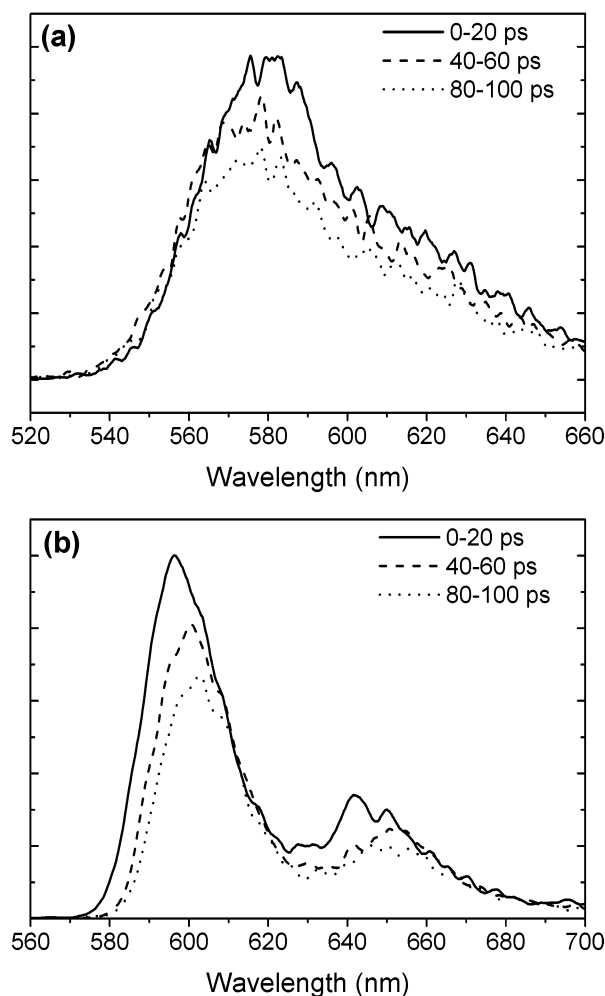


Figure 9. Wavelength dependence of the fluorescence decay at 298 K (a) and 4 K (b). Spectra are produced by summing over consecutive windows with widths of 20 ps.

account vibrational frequency changes between the ground and excited states, as observed in phenylene-ethynylene oligomers.^{47,48} In addition to modeling the vibronic line shape, we would also want to obtain independent measurements of the homogeneous and inhomogeneous line widths to use in energy-transfer modeling. Along these lines, our assumption that the broadening mechanisms can be neatly divided into purely homogeneous and inhomogeneous components may be overly simplistic. Three-pulse photon-echo experiments, similar to studies by Scholes et al.,⁴⁹ may help provide some insight into the different time scales and energies involved in determining the line shape of MEH-PPV. Finally, our calculations do not take the pulse bandwidth into account, which serves to broaden the distribution of excited chromophores and thus the fluorescence spectrum, which would change the initial spectral overlaps.

A final point is that our femtosecond pump–probe experiments only probe the energy transfer that occurs immediately after excitation. Once this initial anisotropy decays, we have no way of probing the subsequent evolution of the energy. The fluorescence spectrum of solid MEH-PPV at 298 K does not undergo an observable shift on the time scale of tens of picoseconds (Figure 9a), but at 4 K, the spectrum shifts continuously over the course of hundreds of picoseconds (Figure 9b). While it is not clear how to separate fluorescence shifting due to intramolecular vibrational relaxation from that due to energy transfer,⁵⁰ it seems likely that at least part of this shifting

is due to energy migration. Other workers have modeled similar time-dependent shifting entirely in terms of exciton diffusion through a manifold of sites to a "localization threshold".⁵¹ Localization occurs when the exciton becomes trapped at a low-energy site because the probability of finding an even lower energy site nearby essentially vanishes. It is possible that this slowing down of the energy transfer at later times is responsible for the γ_0 offsets required to fit our data using eq 4. In this case, the long time constant anisotropy reflects the subdiffusive behavior of the exciton long after photoexcitation, which prevents the complete randomization of the polarization predicted by normal diffusive behavior. Since it is this later time motion that will determine the ultimate range of the exciton motion, it would be beneficial to measure the polarization decay of the excited-state population at various times during its evolution, in addition to the beginning, to determine whether it does indeed slow at later times. If it does, then the diffusion lengths calculated earlier are upper bounds on the true lengths.

Conclusions

Measurements of the steady-state absorption and fluorescence, along with femtosecond degenerate pump-probe experiments at different wavelengths, have been used to investigate energy transfer in MEH-PPV. Both the wavelength dependence of the polarization anisotropy decays and the lack of correlation of the steady-state spectral overlap with the decay dynamics as a function of temperature are in disagreement with the simplest version of Förster theory. Estimating the diffusion length from dynamic as opposed to steady state measurements leads to a 6-fold difference between the two and illustrates the need for more sophisticated treatments. By taking into account an inhomogeneous distribution of absorbers and the intramolecular Stokes shift, we can reproduce the experimental trends. Improvements to this theoretical approach are straightforward and will hopefully lead to a more quantitative description of the data. The hope is that combining line-shape theory with Förster energy transfer, as has been done in the case of biological light-harvesting systems, will provide a predictive understanding of energy transfer in these materials. The work in this paper clearly demonstrates that energy transport in MEH-PPV is dispersive even at room temperature, when one might have expected homogeneous broadening to dominate, and this indicates that the questions of line shape and spectral broadening are important for understanding energy transfer even at the elevated temperatures where actual devices function.

Acknowledgment. Support from the National Science Foundation Grants CHE 99-84683 and CHE 99-82318 is gratefully acknowledged. C.J.B. is an Alfred P. Sloan Fellow.

References and Notes

- (1) McQuade, D. T.; Pullen, A. E.; Swager, T. M. *Chem. Rev.* **2000**, *100*, 2537–2574.
- (2) Friend, R. H.; Gymer, R. W.; Holmes, A. B.; Burroughes, J. H.; Marks, R. N.; Taliani, C.; Bradley, D. D. C.; Santos, D. A. D.; Bredas, J. L.; Logdlund, M.; Salaneck, W. R. *Nature* **1999**, *397*, 121–128.
- (3) Brabec, C. J.; Sariciftci, N. S.; Hummelen, J. C. *Adv. Funct. Mater.* **2001**, *11*, 15–26.
- (4) Forster, T. Delocalized excitation and excitation transfer. In *Modern Quantum Chemistry, Istanbul Lectures*; Sinanoglu, O., Ed.; Acad. Press: New York, 1965; Vol. 3, pp 93–137.
- (5) Forster, T. *Ann. Phys.* **1948**, *2*, 55.
- (6) Czikkely, V.; Forsterling, H. D.; Kuhn, H. *Chem. Phys. Lett.* **1970**, *6*, 207–210.
- (7) Schonherr, G.; Eiermann, R.; Bassler, H.; Silver, M. *Chem. Phys.* **1980**, *52*, 287–298.
- (8) Klafter, J.; Silbey, R. *J. Chem. Phys.* **1980**, *72*, 843–852.
- (9) Haan, S. W.; Zwanzig, R. *J. Chem. Phys.* **1978**, *68*, 1879–1883.
- (10) Godzik, K.; Jortner, J. *J. Chem. Phys.* **1980**, *72*, 4471–4486.
- (11) Jang, S.; Jung, Y.; Silbey, R. *J. Chem. Phys.* **2002**, *275*, 319–332.
- (12) Mukamel, S.; Franchi, D. S.; Loring, R. F. *Chem. Phys.* **1988**, *128*, 99–123.
- (13) Haken, H.; Strobl, G. *Z. Phys.* **1973**, *262*, 135–148.
- (14) Motamedi, F.; Ihn, K. J.; Ni, Z.; Srdanov, G.; Wudl, F.; Smith, P. *Polymer* **1992**, *33*, 1102–1104.
- (15) Chen, S.-H.; Su, A.-C.; Huang, Y.-F.; Su, C.-H.; Peng, G.-Y.; Chen, S.-A. *Macromolecules* **2002**, *35*, 4229–4232.
- (16) Jakubiak, R.; Collison, C. J.; Wan, W. C.; Rothberg, L. J.; Hsieh, B. *J. Phys. Chem. A* **1999**, *103*, 2394–2398.
- (17) Nguyen, T.; Doan, V.; Schwartz, B. J. *J. Chem. Phys.* **1999**, *110*, 4068–4078.
- (18) Lim, S. H.; Bjorklund, T. G.; Gaab, K. M.; Bardeen, C. J. *J. Chem. Phys.* **2002**, *117*, 454–461.
- (19) Wilhelm, T.; Piel, J.; Riedle, E. *Opt. Lett.* **1997**, *22*, 1494–1496.
- (20) Cerullo, G.; Nisoli, M.; Silvestri, S. D. *Appl. Phys. Lett.* **1997**, *71*, 3616–3618.
- (21) Nguyen, T.; Martini, I. B.; Liu, J.; Schwartz, B. J. *J. Phys. Chem. B* **2000**, *104*, 237–255.
- (22) Klopffer, W. Energy Transfer. In *Electronic Properties of Polymers*; Mort, J.; Pfister, G., Eds.; Wiley: New York, 1982; pp 161–214.
- (23) Gochanour, C. R.; Fayer, M. D. *J. Phys. Chem.* **1981**, *85*, 1989–1994.
- (24) Monshouwer, R.; Zarate, I. O. D.; Mourik, F. V.; Grondelle, R. V. *Chem. Phys. Lett.* **1995**, *246*, 341–346.
- (25) Savikhin, S.; Ameongen, H. V.; Kwa, S. L. S.; Grondelle, R. V.; Struve, W. S. *Biophys. J.* **1994**, *66*, 1597–1603.
- (26) Jonas, D. M.; Lang, M. J.; Nagasawa, Y.; Joo, T.; Fleming, G. R. *J. Phys. Chem.* **1996**, *100*, 12660–12673.
- (27) Ma, Y. Z.; Cogdell, R. J.; Gillbro, T. *J. Phys. Chem. B* **1997**, *101*, 1087–1095.
- (28) Gochanour, C. R.; Andersen, H. C.; Fayer, M. D. *J. Chem. Phys.* **1979**, *70*, 4254–4271.
- (29) Knoester, J.; Himbergen, J. E. V. *J. Chem. Phys.* **1984**, *81*, 4380–4388.
- (30) Huber, D. L.; Hamilton, D. S.; Barnett, B. *Phys. Rev. B* **1977**, *16*, 4642–4650.
- (31) Baumann, J.; Fayer, M. D. *J. Chem. Phys.* **1986**, *85*, 4087–4107.
- (32) Nguyen, T.; Wu, J.; Doan, V.; Schwartz, B. J.; Tolbert, S. H. *Science* **2000**, *288*, 652–656.
- (33) Davids, P. S.; Campbell, I. H.; Smith, D. L. *J. Appl. Phys.* **1997**, *82*, 6319–6325.
- (34) Boudrioua, A.; Hobson, P. A.; Matterson, B.; Samuel, I. D. W.; Barnes, W. L. *Synth. Met.* **2000**, *111–112*, 545–547.
- (35) Holzer, W.; Penzkofer, A.; Schmitt, T.; Hartmann, A.; Bader, C.; Tillmann, H.; Raabe, D.; Stockmann, R.; Horhold, H.-H. *Opt. Quantum Electron.* **2001**, *33*, 121–150.
- (36) Greenham, N. C.; Samuel, I. D. W.; Hayes, G. R.; Phillips, R. T.; Kessener, Y. A. R. R.; Moratti, S. C.; Holmes, A. B.; Friend, R. H. *Chem. Phys. Lett.* **1995**, *241*, 89–96.
- (37) Evans, C. E.; Song, Q.; Bohn, P. W. *J. Phys. Chem.* **1993**, *97*, 12302–12308.
- (38) Scholes, G. D.; Jordanides, X. J.; Fleming, G. R. *J. Phys. Chem. B* **2001**, *105*, 1640–1651.
- (39) Hu, D.; Yu, J.; Barbara, P. F. *J. Am. Chem. Soc.* **1999**, *121*, 6936–6937.
- (40) Loring, R. F.; Andersen, H. C.; Fayer, M. D. *J. Chem. Phys.* **1982**, *76*, 2015–2027.
- (41) Reiger, P. T.; Palese, S. P.; Miller, R. J. D. *Chem. Phys.* **1997**, *221*, 85–102.
- (42) Meskers, S. C. J.; Hubner, J.; Oestreich, M.; Bassler, H. *J. Phys. Chem. B* **2001**, *105*, 9139–9149.
- (43) Sperling, J.; Milota, F.; Tortschanoff, A.; Warmuth, C.; Mollay, B.; Bassler, H.; Kauffmann, H. F. *J. Chem. Phys.* **2002**, *117*, 10877–10887.
- (44) Stein, A. D.; Peterson, K. A.; Fayer, M. D. *J. Chem. Phys.* **1990**, *92*, 5622–5635.
- (45) Hagler, T. W.; Pakbaz, K.; Voss, K. F.; Heeger, A. J. *Phys. Rev. B* **1991**, *44*, 8652–8666.
- (46) Chang, R.; Hsu, J. H.; Fann, W. S.; Liang, K. K.; Chang, C. H.; Hayashi, M.; Yu, J.; Lin, S. H.; Chang, E. C.; Chuang, K. R.; Chen, S. A. *Chem. Phys. Lett.* **2000**, *317*, 142–152.
- (47) Gierschner, J.; Mack, H.-G.; Luer, L.; Oelkrug, D. *J. Chem. Phys.* **2002**, *116*, 8596–8609.
- (48) Sluch, M. I.; Godt, A.; Bunz, U. H. F.; Berg, M. A. *J. Am. Chem. Soc.* **2001**, *123*, 6447–6448.
- (49) Scholes, G. D.; Larsen, D. S.; Fleming, G. R.; Rumbles, G.; Burn, P. L. *Phys. Rev. B* **2000**, *61*, 13670–13678.
- (50) Bjorklund, T. G.; Lim, S.-H.; Bardeen, C. J. *J. Phys. Chem. B* **2001**, *105*, 11970–11977.
- (51) Bassler, H.; Schweitzer, B. *Acc. Chem. Res.* **1999**, *32*, 173–182.